Li, Fang; Kõrgesaar, Mihkel; Kujala, Pentti; Goerlandt, Floris

Finite element based meta-modeling of ship-ice interaction at shoulder and midship areas for ship performance simulation

Published in:
Marine Structures

DOI:
10.1016/j.marstruc.2020.102736

Published: 01/05/2020

Document Version
Publisher's PDF, also known as Version of record

Marine Structures 71 (2020) 102736

Contents lists available at ScienceDirect

Marine Structures

journal homepage: http://www.elsevier.com/locate/marstruc

Finite element based meta-modeling of ship-ice interaction at shoulder and midship areas for ship performance simulation

Fang Li [a,*], Mihkel Kõrgesaar [b], Pentti Kujala [a], Floris Goerlandt [c]

[a] Aalto University, School of Engineering, Department of Mechanical Engineering, Marine Technology, P.O. Box 14100, Aalto, FI, 00076, Finland
[b] Tallinn University of Technology, Estonian Maritime Academy, Tallinna 19, Kuressaare, Estonia
[c] Dalhousie University, Department of Industrial Engineering, Halifax, Nova Scotia, B3H 4R2, Canada

ARTICLE INFO

Keywords:
Hip-ice interaction
Ship performance in ice
XFEM
Neural network
Cross-scale modelling

ABSTRACT

The climate change has made the transit through Arctic area more feasible, which demands reliable methods to evaluate ship performance. Ship performance in ice is a cross-scale problem, where the desired output such as ship speed lies in larger scale while the actual ship-ice interaction happens in smaller scale. Due to insufficient knowledge in ice mechanics and the demand for computational efficiency, existing approaches for modelling ship-ice interaction from ship performance perspective are mostly either (semi-) empirical, or simplified analytical, with reduced dimensions and extensively simplified mechanics. This paper presents a novel approach to model ship-ice interaction, which maintains the accuracy of the modelling with Finite Element Method (FEM) in ship-ice interaction scale, while being computationally very cheap, therefore is capable to be applied in ship scale simulations. The ice failure is firstly qualitatively investigated through full-scale and model-scale observations, as well as a numerical simulation with Extended Finite Element Method (XFEM). The model is then simplified and executed by Abaqus to automatically run a large database. A neural network is used to fit the results to get a simulation-free tool for ship-ice interaction calculation. Finally, the uncertainty in the results due to an important assumption is quantified. The results show that the obtained neural network fits the database with excellent performance. Therefore, it can be applied in ship scale simulations with improved accuracy compared to empirical or analytical approaches.

1. Introduction

Safe and efficient shipping activities through ice-covered areas relies on both accurate forecasts of ice conditions and a reliable prediction of ship performance along the route. This paper focuses on the latter. Ship resistance in various ice conditions is the core issue in predicting ship speed and therefore voyage time. Many efforts have been devoted in finding proper ways to predict ship resistance, e.g. Lindqvist [1] and Riska et al. [2] representing semi-empirical formulae; Lubbad and Løset [3] representing numerical simulations. Semi-empirical formulae have the advantages of easy implementation and fast calculation, while numerical simulations are able to account for more ship details with more flexible ice configuration, which potentially lead to better accuracy [4]. Motivated by this, several numerical models have been developed to simulate ships going through ice (e.g. Lubbad and Løset [3] for level ice; Gong et al. [5] for ridged ice; Sorsimo et al. [6] for channel ice; Lubbad et al. [7] for pack ice).

* Corresponding author.
E-mail address: fang.li@aalto.fi (F. Li).

https://doi.org/10.1016/j.marstruc.2020.102736
Received 26 August 2019; Received in revised form 5 January 2020; Accepted 21 January 2020
Available online 21 February 2020

The selection of methods differs according to actual needs. For example, semi-empirical formulae are preferred in operability assessment [8] and route optimization [9] due to the fast calculation where numerical simulation is impractical. In other cases, such as ship design where proper hull form needs to be determined optimize performance, numerical simulation has a potential to become a powerful tool [10].

Most existing numerical models for ship performance simulation are not fully mechanics-based, i.e. they do not numerically simulate the stress and crack evolvement. The interaction is usually simplified into a semi-infinite wedge with forces exerted on the edge and then calculated either with semi-empirical or analytical formulae (e.g. Lubbad and Løset [3]; Su et al. [11]). The obtained formulae are then applied as the criteria for ice failure in the models for ship performance simulation. One of the greatest drawbacks of such approach is the inaccuracies in ship-ice interaction scale that are caused by the excessive simplifications, which are needed to use semi-empirical and analytical formulae. However, this approach is favored by many researchers, mainly because of the computational need and the lack of knowledge in fundamental ice mechanics.

This paper aims to find a way to fill the gap between the ship-ice interaction scale and ship scale, in order to maximize the knowledge passed from the modelling in local (ship-ice interaction) scale to global (ship) scale with negligible additional computational cost. The case under investigation is the ship-ice contact at bow shoulder and stern shoulder, as well as at midship area. These are most relevant for a ship turning in level ice or a ship encountering converging ice field, where considerable contact may occur at shoulder and midship areas. This case differs from the interaction at bow area on the fact that, the ship hull at bow shoulder and midship area is typically vertical or close to vertical, thus the in-plane force is much larger than the out-of-plane force. The aforementioned analytical or semi-empirical methods are mostly proposed assuming negligible in-plane force, therefore the premises do not hold in our present case. A new model is called for.

The following procedure is followed during the investigation process. Section 2 starts with an overview of the problem under investigation, upon which the methodology (developed in Section 3) used to proceed the investigation is based. In Section 4, a qualitative investigation into the failure mode is conducted, first by full-scale and model-scale observations to identify the key relevant issues to model, and then by an FE model aiming to qualitatively capture the observed phenomena. Following that, in Section 5, a large number of simulations are run to generate considerable amount of results, with which an advanced fitting technique is used to fit the results so the results can be expressed in a simple form for fast calculation in ship scale simulations. The final step in Section 6 is to quantify the uncertainties lying in the results due to an important assumption. Following this procedure, a neural network is eventually set up together with quantified uncertainty. The neural network is attached as the supplementary material to this paper for anyone interested to use. The discussion is presented in Section 7 and finally Section 8 concludes.

2. Background

There are typically three scales in issues related to a ship in ice, namely:

a. Ice forecast scale, with length to the magnitude of grid cell width (e.g. 1 nm for HELMI model from Finnish Meteorological Institute [12]), where ice information such as concentration and thickness is given for each grid cell. Issues such as voyage planning are concerned.
b. Ship scale, with length to the magnitude of ship length (order of 10^1–10^2 m), where ship performance issues such as resistance, speed, and maneuverability are dealt with.
c. Ship-ice interaction scale, with length to the magnitude of a single ship-ice contact (order of 10^{-1}-10^0 m), where issues such as ice loads and structural response are in focus.

Considering the above, safe and efficient ship operation in ice relies on.

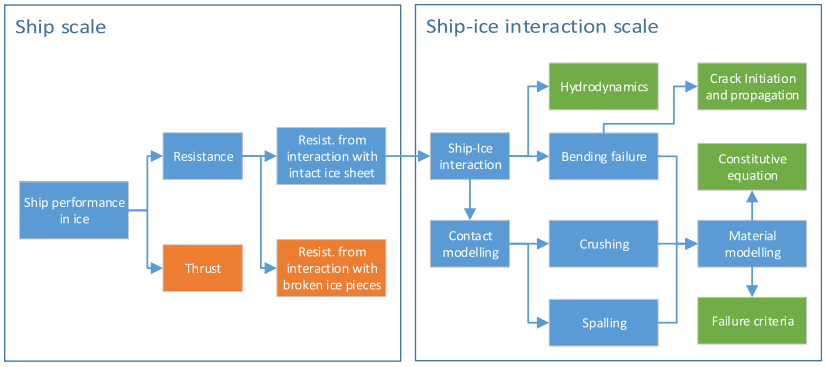

Fig. 1. Decomposition of ship performance in ice problem. The orange blocks are out of the scope of this paper. The green blocks are the fundamental problems, while the blue are in upper levels. (For interpretation of the references to colour in this figure legend, the reader is referred to the Web version of this article.)

a) accurate forecast of ice conditions;
b) good understanding of ship performance in various ice conditions; and
c) reliable estimation of ice loads on the ship hull.

The first point concerns ice forecast and is out of the scope here. The second point is tightly connected to the third point, since ship resistance is the summation of each individual contact force in ship-ice interaction scale. Therefore, ship performance in ice is a cross-scale problem, where the interaction takes place in local scale while the parameters of interest lies in global scale. This paper aims to deliver a model dealing with a ship-ice interaction scale issue, but meanwhile being computationally efficient to be applied in ship scale simulations. This section gives an overview of the background information in both ship scale (Section 2.1) and ship-ice interaction scale (Section 2.2). The overview aims to analyze the problem breakdown and conclude the state-of-art knowledge in both scale, which forms the fundaments of Section 3 to develop the suitable methodology.

2.1. Ship performance in ice: problem decomposition and scope

Ship performance in ice deals with ship resistance, maneuverability and propulsive performance in ice. It is an engineering problem consisting of various elements. Fig. 1 presents a breakdown of typical ship performance in ice problem. The two main components are the available thrust in ice to overcome ice resistance, and the forces (resistance) a ship receives from the interaction with ice, both in straight course and during turning. Ship resistance is the summation of each individual contact force between the ship and the ice, resulting from crushing and cracking the ice as well as turning and clearing the ice pieces. The modelling of these elements relies on both deep understanding of ice mechanics, including correct material modeling of ice constitutive equation and modeling of ice fracture, as well as accurate modelling of the ice dynamics including the interaction between the discrete ice pieces, the ship and water with hydrodynamic effects. However, most of these modelling works have not progressed onto a stage where systematic validation has taken place and a widely accepted model is readily applicable. This leads to the fact that most of the methods in practical use to estimate ship resistance in ice are accompanied with empirical factors, obtained through curve fitting of existing data from full-scale measurements (e.g. Lindqvist [1]). The authors believe the empirical approach will continue playing an important role in ship performance estimation until adequate progress has been achieved to model the problems in Fig. 1 with first-principle approaches.

The problem dealt with in this paper is the ship-ice interaction under the context of a ship turning in level ice or going through a converging ice field. In these cases, due to the relative motion between ship and ice in the lateral (orthogonal to ship speed) direction, the shoulder and midship area get into considerable contact with the ice sheet. Higher ice forces are exerted on these areas compared to a ship going through a static ice field in straight course [13]. The ship then endures additional resistance, which dampens ship turning or reduces the ship speed in a converging ice field. Some example of models dealing with these issues includes Su et al. [11]; Liu et al. [14] for ship turning in ice and Külaots et al. [15] for converging ice field. These are numerical models adopting semi-empirical formulae for ship-ice interaction modelling.

2.2. Ship-ice interaction: review of modelling approaches and focus of the paper

Estimation of ship performance relies on modelling of ship-ice interaction. A simple example is the level ice resistance formula by Lindqvist [1], where the force to cause ice failure by bending during one contact is taken to be $0.5\sigma_b h^2$, with σ_b being the flexural strength and h the ice thickness. The length of the broken ice pieces is taken to be one third of the characteristic length lc, without further justification. While being simple, these expressions build the link between a single contact in local scale and the global load (resistance) in global scale, and enable an analytical expression for resistance estimation. However, the process happening during ship-ice interaction is then significantly simplified. An accurate numerical model for ship scale simulation with wide applicability for different hull forms and maneuvering relies on more accurate modelling of ship-ice interaction. This paper aims to construct a model capable of giving more accurate results for ship-ice interaction, with high simplicity in expression to be used for ship performance estimation.

Following Fig. 1, modelling of ship-ice interaction involves the modelling of the crushing, spalling, bending and splitting failure, which rely on several fundamental aspects such as constitutive modelling and fracture modelling. Constitutive modeling of ice for ice-structure interaction analysis is a challenging task. The physically based ice material models (e.g. Kolari [16]) emphasize the description of internal microscopic changes of ice, but are still at the initial stages and need further experimental research of the micromechanics. Phenomenological ice material models (e.g. Liu et al. [17]; Xu et al. [18]) based on the theory of viscoelasticity/-plasticity are easy to implement, but need extensive experimental validation due to the lack of scope on the microscopic scale and are still largely empirical with coefficients to describe e.g. the failure strain. Phenomenological ice material models are normally applied to model ice crushing against a structure, and are usually validated via comparing with standard pressure-area relationship curve (e.g. Xu et al. [18]). This, however, implies that the pressure-area relationship curve is still a state-of-the-art method in practice to define the crushing pressure and force. This further indicates that at the current stage, numerical simulation of ice crushing may not lead to added value compared to a pressure-area relationship for those problems where the pressure distribution inside the contact area does not have vital influence on desired outcome.

Ice fracture in the context of ice-structure interaction mainly refers to the splitting and bending failure of ice. Some recent models (e.g. Lu et al. [19,20]) apply Linear Elastic Fracture Mechanics (LEFM) to calculate and simulate crack propagation in ice. According to Lu et al. [21], the typical modelling approaches for crack propagation includes FEM with element erosion technique, cohesive element method (CEM), the discrete element method (DEM) with cohesive contacts and the extended finite element method (XFEM). One of the

most important parameter in modelling cracks is the fracture toughness. According to Timco and Weeks [22], the Mode-I fracture toughness K_{1c} of sea ice has been relatively more measured compared to those in other fracture modes, e.g. by Dempsey et al. [23], but the size effect still needs further study.

The ship-ice interaction in the scope of this paper deals with the interaction between an ice sheet and a moving hull. The hull inclination angle at shoulder and midship area is typically in the range of 0–10°. Naturally, the key features of this type of interaction are:

a. The in-plane force is much larger than out-of-plane force, due to the small hull angle.
b. The interaction speed is low, typically below 1 m/s in full-scale.
c. Ice pieces may pile on and below the ice sheet, but the extent is not significant due to ship movement.
d. The structure (ship) is moving in tangential direction, which is approximately orthogonal to the relative speed between ship and ice.

This kind of interaction then differs from typical ship-ice interaction at bow area on the first two points of the above features. At bow area, the interaction speed is much larger (typically above 1 m/s), therefore the hydrodynamic force and ice inertial can play an important role. Moreover, the out-of-plane force is much larger at bow area since the ship hull there is more inclined, which might be the reason that many models (e.g. Lubbad and Løset [3]) simply neglect the in-plane force. At shoulder and midship areas, the hydrodynamic force might be less an issue, but the in-plane force is so large that it is questionable to be simply neglected. Therefore, models primarily proposed for bow regions may not well predict the interaction at shoulder and midship area. The interaction also differs from typical offshore structure-ice interaction, where the structure is fixed or moored and considerable ice pieces can pile against the structure [24]. To the authors' knowledge, there have not been models specifically designed for this type of ship-ice interaction.

3. Methodology

With the complexity in the problem as analysed in Section 2.1 and the unknown fundamental knowledge as stated in Section 2.2, the modelling of ship-ice interaction for ship scale applications is a challenging task, which needs a proper methodology to simplify the problem while keeping the key elements. It is not practically realistic and computationally efficient to model all the elements in Fig. 1, especially with the lack of fundamental knowledge on ice mechanics. In the context of modelling ship sailing through ice, it is preferred not to spend much computational power on each individual interaction since the scenario may involve a huge number of interactions.

Therefore, in this paper, the methodology presented in Fig. 2 is adopted during the whole modelling process. The starting point is the observations from full-scale and model-scale tests, which helps to understand different phenomena and identify the ones relevant for accurate modelling. Following this, a numerical model is set up to capture the critical phenomena. Despite of applying the advanced numerical method, the aim is to get qualitative conclusions on ice failure in order to understand the factors influencing the failure process. The observations provide visual evidence, while the simulation compensates the limited information conveyed from observations and provides theoretical insights into the phenomena. After the qualitative investigation, quantitative modelling takes place by running a large set of cases to effectively generate a database, which is then further used to obtain a generalized function to replace the simulation with fast calculation. The last step is to quantify the uncertainties underlying one important simplification, so that the uncertainty quantification can be incorporated into the developed model.

4. Observation and qualitative investigation

This section starts with problem identification via full and model scale observations. The dominating ice failure mode is identified

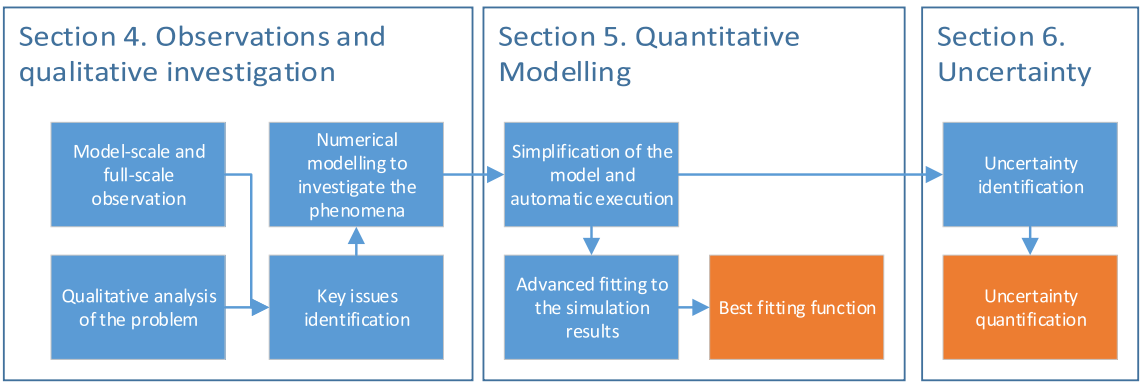

Fig. 2. Flowchart of the problem-solving process. The blue blocks are the modelling processes and orange blocks contain the outcome of this work. (For interpretation of the references to colour in this figure legend, the reader is referred to the Web version of this article.)

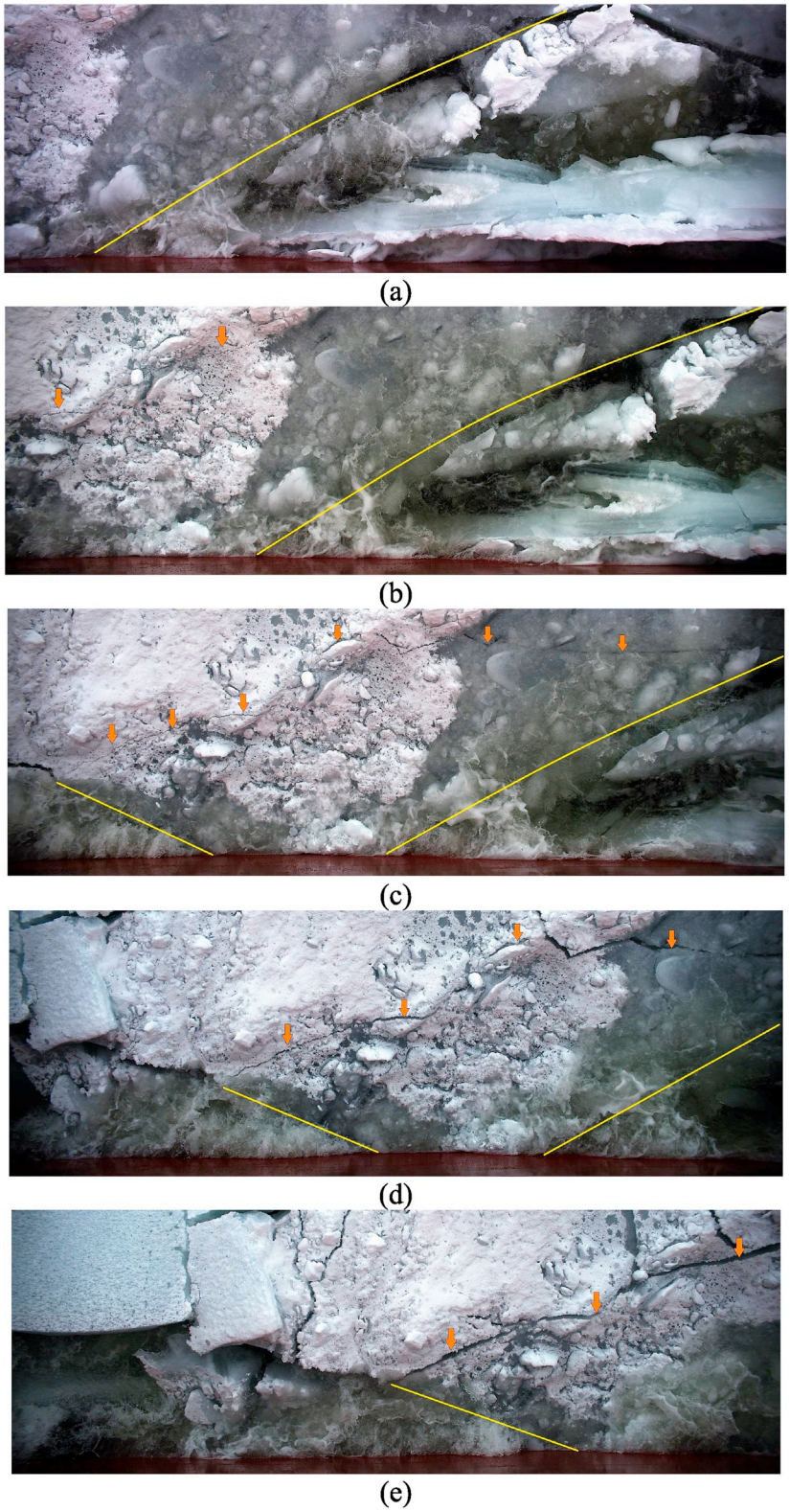

Fig. 3. Ice bending failure at bow shoulder area during turning of S.A. Agulhas II, taken by a stereo camera. The yellow lines illustrates the ice edge and the orange arrows point out the crack location. The time interval between the photos is 1/3s. a) Before crack initiation; b) crack initiated and in propagation on the top surface; c) crack propagated through the top surface; d) crack opening; e) crack further opening, ice leaves the scope of the camera. (For interpretation of the references to colour in this figure legend, the reader is referred to the Web version of this article.)

from photos and videos shot at certain ship regions during ice tests. Following that, XFEM is applied to analyze the bending failure. XFEM is selected because of its mesh-independency, allowing crack initiation and growth through the elements. As will be shown in this section, the XFEM simulation does not achieve full success due to the difficulties in propagating the crack through the thickness. The focus is then restricted to gaining insights in the crack propagation on the top surface. In spite of the restriction, the obtained results already present considerable insights into the failure process, therefore presented here in detail.

4.1. Full-scale and model-scale observations

The first source of observation comes from the ice trial of the polar supply and research vessel S.A. Agulhas II on the Baltic Sea in 2012. The instrumentation and measurement on this vessel have been presented in several articles, e.g. Suominen et al. [25]; Kotilainen et al. [26], and therefore is not repeated here. During the voyage, several maneuvering tests were conducted in controlled conditions. On 21st March, the ship made a turning test in selected level ice. A stereo camera installed at bow shoulder area made observations directly downwards onto the ice sheet and took photos in 3 Hz; see Li et al. [27] for more information on the stereo camera system and analysis of the photos. The photos show clearly that during the ship turning, bending failure happens consecutively at the bow shoulder area. Fig. 3 presents an example of the photos showing the development of a typical bending crack when the ship was turning starboard. The crack initiated and propagated across the top surface and then through the thickness during this approximately 1.33s segment.

The second source comes from an overview and preliminary analysis of a ship going through a compressive ice channel (also called converging ice); see Li et al. [28]. In this paper, two previous projects regarding ships in compressive ice are used as references. The model scale tests in both projects were conducted in Aalto University (previously Helsinki University of Technology) Ice Tank. Li et al. [28] summarised the tests and showed that there is considerable bending failure at midship area (see Fig. 4), although the ship hull at midship area is vertical. Therefore, crushing-bending dominates the failure mode. The bending failure may be due to the hull motion, the piled ice pieces and the eccentricity in the contact area.

It can be concluded that in both cases, the existence of the bending failure is evident. The bending failure plays a determining role in the maneuverability during turning and operability in a converging ice field, since bending failure releases the continuous crushing force and turn the intact ice-ship contact into discrete ice-ship contact. The correct modelling of the crushing-bending failure at shoulder and midship areas may determine whether a ship with relatively long parallel midbody is able to turn in level ice or go through a converging ice field due to extensive additional resistance. The model proposed in this work focuses on such ice failure.

4.2. Modelling bending failure with XFEM

4.2.1. Basics on XFEM

Extended Finite Element Method (XFEM) is a relatively new method to model crack initiation and propagation in materials [29]. XFEM is theoretically a mesh-independent method, which allows the crack to propagate through the element without remeshing. This is achieved by enriching the solution space for solutions to differential equations with discontinuous functions. Lu et al. [21] applied XFEM to model ice bending problem and came to the conclusion that XFEM is a promising method to model crack propagation but is in its developing stage, with still some practical issues to fix. In Abaqus/Standard 2017, XFEM is an available technique allowing the modelling of crack growth using either cohesive segment method or linear elastic fracture mechanics (LEFM). In this paper, XFEM with LEFM is used.

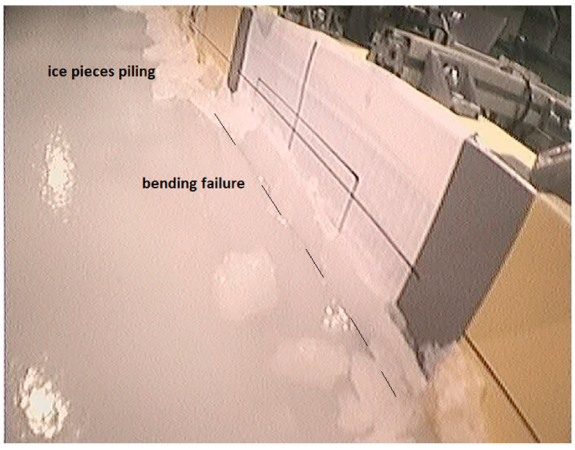

Fig. 4. A typical bending failure when a ship is moving in a compressive ice channel. The black dashed line illustrates the bending crack location (Source: Li et al. [28]).

4.2.2. Assumptions and simplifications

The primary goal of the XFEM modeling is to identify and characterize the bending cracks as described in Section 4.1, because of their importance in ship performance modelling. As illustrated in Fig. 1 and discussed in Section 2.2, modelling ship-ice interaction involves at least the modelling of crushing and the hydrodynamic effect in addition to bending. While being also relevant in ship-ice interaction, the crushing process and hydrodynamic effect are simplified or neglected according to the following reasons.

The hydrodynamic effect is neglected and the water is modelled as an elastic foundation. It is known that the hydrodynamic effect plays an important role during ship-ice contact in the bow region [30]. However, at shoulder and midship area where the ship hull is vertical or close-to vertical, the vertical component of the relative speed between ship and ice is very small. Keijdener et al. [31] analysed the failure of an ice beam floating on water interacting with sloping structures. The results show that the hydrodynamic force starts to become important when the ice moving speed is larger than a transition velocity. Considering that analysis was conducted in two dimensions, where the water is more confined compared to three-dimensional reality, the actual transition velocity might be higher. Based on these arguments, the effect of hydrodynamic force for the analysed case is deemed small, and thus neglected.

The second simplification deals with the modeling of pressure on the nominal contact area due to ice crushing. As reviewed in Section 2.2, the pressure-area curve is still the most practical tool to describe the nominal ice pressure on a certain area, despite of the extensive efforts devoted to model this problem. It is then questionable whether a more complex model (e.g. by modelling the actual contact and by using a designed material model) could give more credible results on the pressure magnitude and distribution in the nominal area. Moreover, the location of the bending crack is usually not in the vicinity of the contact area. Therefore, the pressure distribution inside the contact area is presumed to have little influence on the bending crack according to Saint Venant's Principle. Consequently, the pressure is assumed to spread uniformly on the contact area. The modelling of contact and ice crushing are then not needed, which significantly reduces computational effort.

4.2.3. XFEM model configuration

Ship-ice interaction has commonly been modelled as a rigid plane interacting with a wedge with certain wedge angle θ. The simplification of ice sheet as an infinite wedge enables analytical solution (e.g. Nevel [32]) or semi-empirical approximation (e.g. Su et al. [11]), but the validity of the simplification needs to be examined. As illustrated by Fig. 5, the actual geometry of the ice sheet is more like a finite wedge connected with a large sheet. The wedge analogy may be valid if the wedge depth b is much larger compared to the contact length c. However, for the present case, the bending failure may occur after quite large indentation into the wedge (therefore gives large c and small b) since the out-of-plane force is much smaller than the in-plane force. The wedge analogy may not be valid anymore and thus likely cannot give a good approximation. Therefore, the ice geometry in Fig. 5 is applied to better reflect the reality, which is a composition of a wedge and a plate, similar to the FE configuration by Varsta [33]. The geometry is characterized by the wedge depth b, contact length c, ice thickness h, and wedge angle θ. The curve of the wedge edge is modelled as an arc, therefore a can be calculated from b and θ. The black solid line on the top surface separates the region where the mesh is refined, and is also the enriched region where XFEM is implemented. The mesh is further refined near the loading area.

The contact and bending failure is modelled as follows. A uniformly distributed pressure is exerted on the contact surface. The total contact force is set to increase linearly as a function of time with the rate approximately equivalent to an indentation speed of 0.5 m/s into the wedge. In addition to the in-plane normal force N in positive y-direction, there is an in-plane tangential force f in positive x-direction to model the friction ($f = \mu_2 N$) and an out-of-plane force P ($= \mu_1 N$) in negative z-direction. The water is modelled as an elastic foundation. The size parameter d of ice sheet is set large enough that it does not affect the output. The ice sheet is constrained in the far side to prevent movement in y- and x-direction.

The model is built in Abaqus/Standard, which adopts implicit methods to simulate. The initial time increment and maximum time increment are set small enough so that multiple cracks do not show up in one time step. The crack initiation criterion is set to be the maximum principal stress exceeding a limit value (here the flexural strength is used because of its wide application in engineering problems). The ice sheet is set to be pure elastic, but with an elastic modulus gradient through the thickness. The varying modulus through thickness is known to be a common feature of sea ice [34] and some model ice [35]. The elastic modulus is set to be highest in

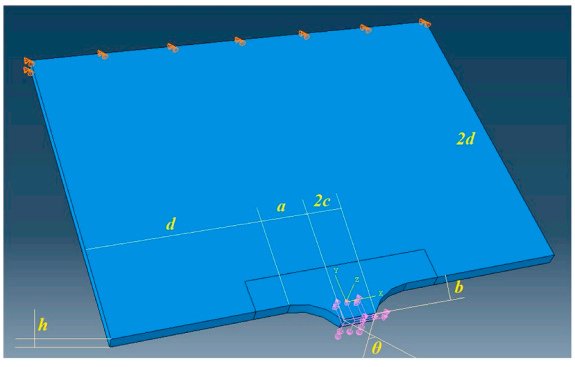

Fig. 5. Geometry of the model ice sheet (not drawn to scale). The pink arrows show the force direction and orange cones illustrates the boundary conditions. (For interpretation of the references to colour in this figure legend, the reader is referred to the Web version of this article.)

the top surface (twice of the mean modulus across the thickness) and decrease along the thickness direction. The effect of elastic modulus profile will be elaborated in Section 6. Table 1 summarizes the parameters used in the simulation. Two cases with different contact geometry and force coefficients are investigated.

4.2.4. XFEM results

Fig. 6 presents the process of crack initiation and propagation through the top surface. The distribution of maximum principal stress before crack initiation is shown in Fig. 6a, where the maximum value of the maximum principal stress (hereafter referred to as 'bending stress' for simplicity) is located close to the edge. In Fig. 6b, at t = 241.9 ms, the crack appears in the element where the bending stress exceeds the threshold. The crack then propagates mainly on the top surface of the ice sheet and at t = 332.9 ms, it reaches the other edge (Fig. 6c). However, the further crack propagation through the thickness encounters major problems in our simulation. The crack goes through the elements in thickness direction for a while but always failed to penetrate through the bottom surface. The crack becomes rather irregular and the simulation then fails at one moment when two cracks meet each other, which the current XFEM cannot handle. Due to this defect, the simulations are ended once the crack has fully propagated through the top surface.

It is worth noting that it takes some additional time from the moment of crack initiation to the full propagation through the top surface, indicating that additional energy is needed to complete the process. This is likely due to the existence of the in-plane force, which dampens the crack propagation. To confirm this, two more simulations are run with the same out-of-plane force but different in-plane force (i.e. different μ_1), one with μ_1 equaling 0.1 and the other equaling 1. The time instances when a crack is initiated and propagated are listed in Table 2. It shows clearly that with a larger in-plane force, $t_{propagated}/t_{initiate}$ gets larger, indicating that more energy is needed to propagate the crack after initiation. When the in-plane force equals the out-of-plane force, the crack propagates quickly through the top surface after the initiation within 40 ms, implying minor influence of in-plane force in this case. This indicates a major difference between the interaction at ship bow area and shoulder or midship area.

The maximum principal stress distribution before crack initiation and the propagated crack in case 2 are shown in Fig. 7. In this case, the crack initiates at $t_{initiate} = 675.2ms$ and propagates through the top surface at $t_{propagated} = 1128ms$. The ratio $\frac{t_{propagated}}{t_{initiate}}$ is 1.67, higher than case 1 with $\mu_1 = 0.1$. This is likely because that in case 2, the wedge depth b is smaller while the contact length c is larger. As illustrated in Fig. 7a, there are three regions in the path of the crack propagation. In region I, the crack initiates and propagates easily without requiring much additional energy. In region II, due to the influence of the in-plane force, much energy is needed to propagate the crack. Once the crack leaves region II and enters region III, it again propagates quickly until reaching the edge. The parameters b and c determine the extent of influence from the in-plane force, thereby influencing the energy needed to propagate the crack.

Another issue of interest is whether the inertia of ice significantly affects the bending failure. To investigate this, both case 1 and case 2 are run with quasi-static loading (see Table 1 for pressure increasing rate), i.e. without inertia term. The new runs result in very similar cracks as obtained with the dynamic loading. The time instances of crack initiation and completed propagation are 233.5 ms and 358.4 ms in case 1, and 633.5 ms and 1285 ms in case 2. Compared to dynamic cases, the crack initiates slightly earlier with quasi-static loading and needs slightly more additional energy (11% and 17% more in terms of $\frac{t_{propagated}}{t_{initiate}}$) to propagate through the top surface. However, the difference is relatively small, indicating that with interaction speed approximately 0.5 m/s, the ice inertia does not have major influence on the failure process.

4.2.5. Discussions on the XFEM simulation results

The modelling results using XFEM in the previous section succeed in capturing the bending failure observed in the full-scale and model-scale tests. The results give information regarding the progress of the bending crack. A short summary of the findings is given below, which will be the theoretical basis of the following sections.

First, maximum principal stress as the failure initiation criterion and LEFM as crack propagation criterion captures the observed bending crack. The crack starts close to the edge at the top surface and propagates through the top surface. Considerable additional energy may be required to propagate the crack through the top surface due to the existence of in-plane force. The problem can then be divided into two parts: the moment of crack initiation and the energy needed to propagate a crack. The former can be numerically

Table 1
Parameters in XFEM simulation.

Quantity	Notation	Case 1	Case 2
Ice thickness	h	0.3 m	
Ice density	ρi	900 kg/m^3	
Elastic modulus	E	5 GPa	
Flexural strength	σ_f	400 kPa	
Energy release rate	G	5J/m^2	
In-plane nominal pressure	p	1 MPa/s*time	1.732 MPa/s*time
Other force coefficients	(μ_1, μ_2)	(0.2, 0.1)	(0.1, 0.1)
Contact geometry	(b, c, θ)	(2.4 m, 0.6 m, 90 deg)	(1.8 m, 0.9 m, 120 deg)
Ice sheet size	2d	120 m	120 m
Max. time increment	δt	2 ms	2 ms

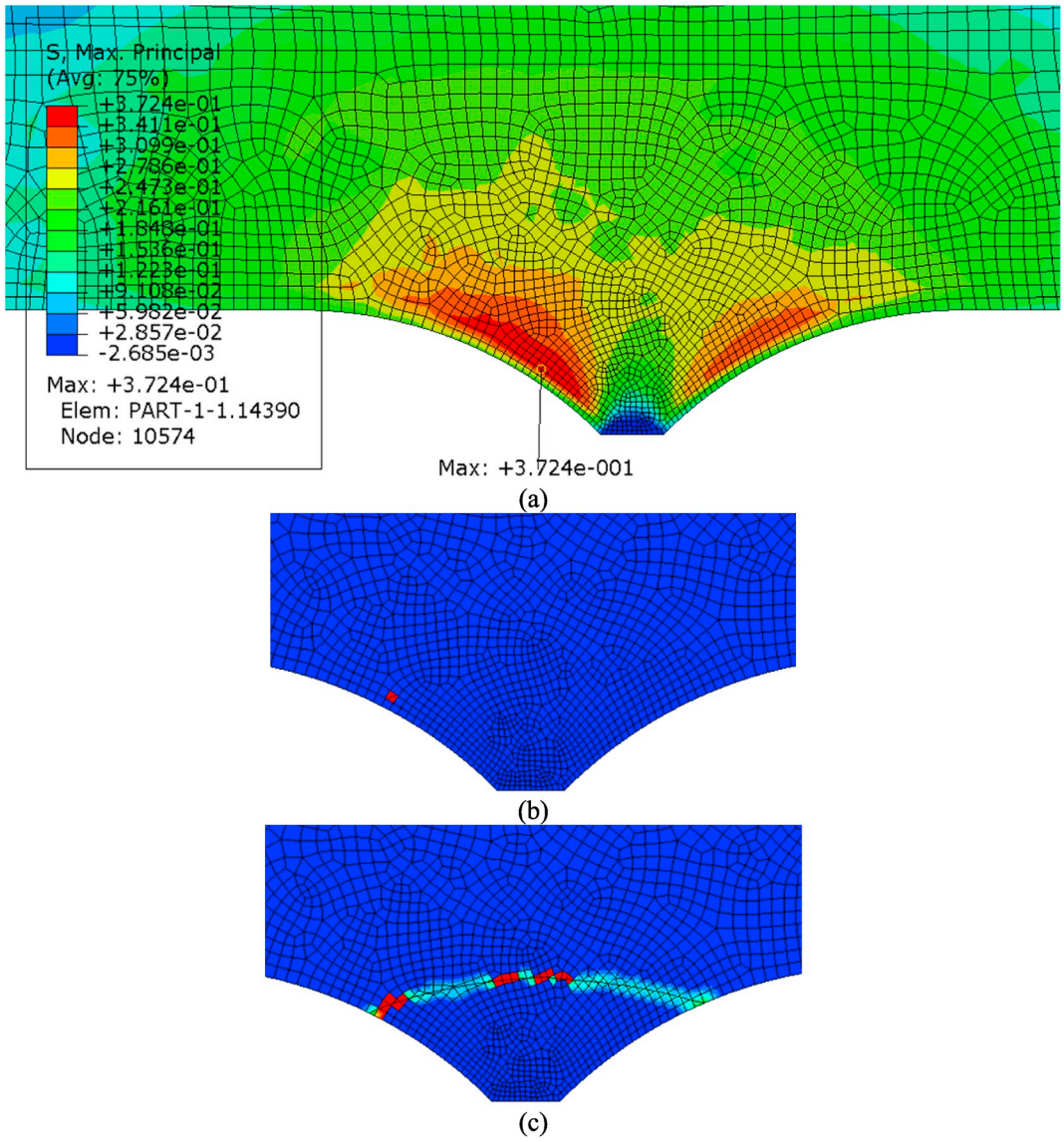

Fig. 6. Maximum principal stress distribution (a), crack initiation (b) and propagation (c) in case 1; see Table 1 for the parameters.

Table 2
Moments of crack initiated and propagated through the top surface.

$1/\mu_1$	10	5 (case 1)	1
$t_{initiate}$	255.3 ms	241.9 ms	242.6 ms
$t_{propagated}$	398.2 ms	332.9 ms	280.0 ms
$t_{propagated}/t_{initiate}$	1.56	1.38	1.15

calculated without simulating the crack, which is the focus of the next section. The latter, while being also important, is still difficult to quantify numerically and is left for future research.

Second, the interaction speed (0.5 m/s) is low enough that quasi-static modelling gives rather similar crack initiation time with dynamic modelling. This suggests that when focusing on the bending stress, quasi-static modelling can replace dynamic modelling. The main benefit of quasi-static modelling is that, the interaction process can be discretized into independent moments. The stress distribution at different moments are then history-independent and therefore can be numerically calculated individually.

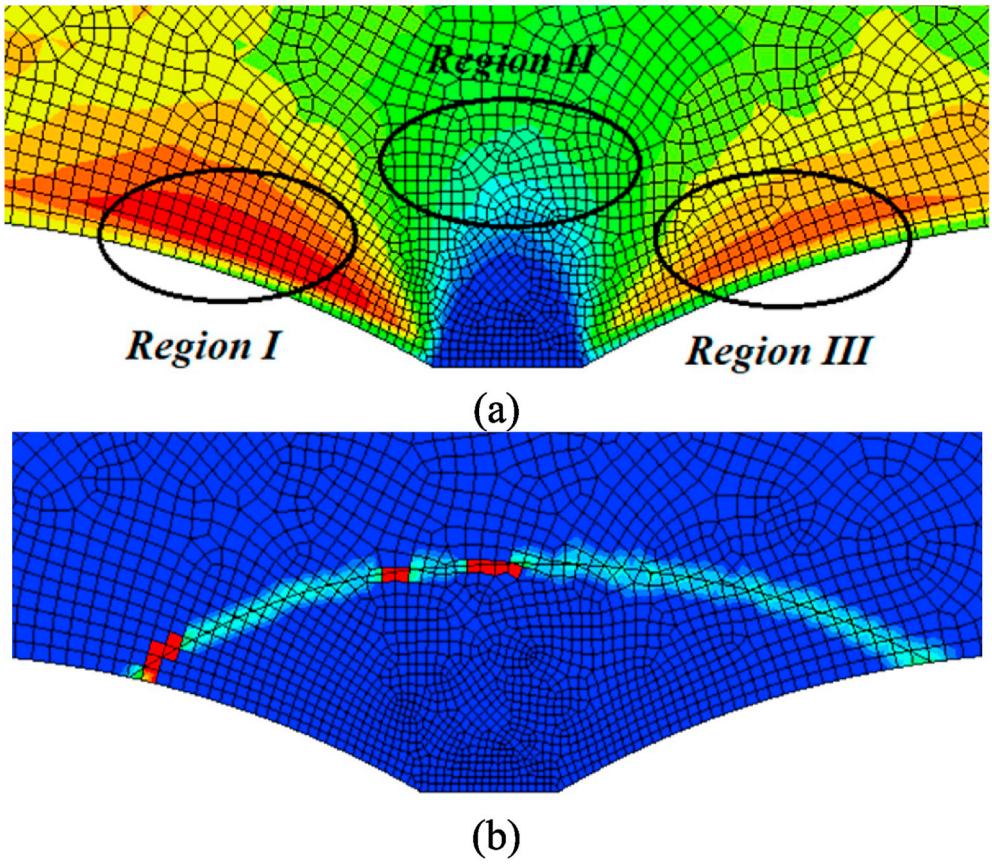

Fig. 7. Maximum principal stress distribution (a) and crack (b) in case 2; see Table 1 for the settings.

5. Meta-modeling of ship-ice interaction

As discussed in Section 4.2.5, this paper focuses on the ship-ice interaction process until crack initiation, with no need for actual simulation of cracks. FEM can reasonably calculate the stress field evolvement during the indentation, but is computationally inefficient for simulations in ship scale. This section aims to develop a model which has the simplicity of analytical formulae, while being based on and thus as accurate as FE simulations.

Meta-modeling can be a good approach for cross-scale problems to maintain the accuracy of local scale simulations, while being computationally inexpensive in global scale. Meta-modeling can be used for studying the input and output relationships by fitting right meta-models to represent that behavior. The analytical solutions (e.g. Nevel [32]) can also be regarded as a simple type of meta-model, which links the input (contact force, ice geometry, ice properties) to output (stress in the field, location of the bending failure) with idealized interaction scenarios. In this paper, a novel meta-model is built using FE simulations and advanced fitting technique to link the input and output, in order to keep the accuracy in the meta-model.

In Section 4.2, the ice sheet was assigned an elastic gradient through thickness to mimic sea ice in reality. However, the extent of actual elastic modulus gradient is difficult to quantify and largely dependent on the ice formation process and the air temperature. Due to this uncertainty, here the issue with elastic modulus gradient is separated into two parts. In this section, the elastic modulus is set to be a constant through the thickness to avoid subjectivity, and then in the next section, the uncertainty arising from different extent of elastic modulus gradient is quantified.

5.1. Parameterization of the problem

The first step of the meta-modeling is to parameterize the problem so that the input and output can be easily defined with several parameters. The same geometry presented in Fig. 5a is adopted to model the ice field and is re-presented in Fig. 8 for further explanation. The contact is characterized by a set of non-dimensional parameters: b/l_c for the wedge depth, c/l_c as the contact length, θ as the wedge angle, μ_1 as the ratio between the out-of-plane force and the in-plane normal force, and μ_2 as the friction coefficient for the in-plane friction force. Here l_c refers to the characteristic length calculated by $\sqrt[4]{\frac{Eh^3}{12\rho g(1-\nu^2)}}$. It is a parameter commonly applied (see e.g. Nevel [32] for the derivation) to non-dimensionalize the governing equation of an elastic plate resting on elastic foundation. The

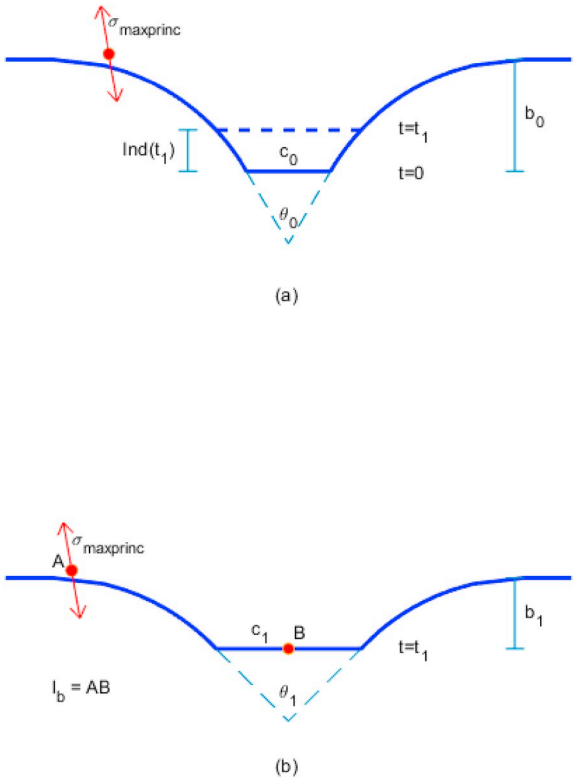

Fig. 8. Illustration of the indentation process. *Ind(t1)* denotes the indentation depth at time *t1*; the red arrows show the direction of maximum principal stress; the blue dashed line the contact surface at time *t1*; *lb* the potential breaking length. (For interpretation of the references to colour in this figure legend, the reader is referred to the Web version of this article.)

desired outputs relevant for bending failure are the maximum value of the maximum principal stress $\sigma_{MaxPrinc}$, which tells whether a crack will be initiated, and the location of this stress, from which the size of the broken ice piece can be approximated. The location of $\sigma_{MaxPrinc}$ is expressed in the output by a breaking length l_b, which is the distance between the location of $\sigma_{MaxPrinc}$ and the center of contact area (see Fig. 8). These are important parameters for ship performance simulation.

The idea is to model the ship-ice interaction as illustrated in Fig. 8. At t = 0, a ship gets into contact with an ice sheet, with force parameters μ_1, μ_2 and initial geometrical parameters θ_0, b_0 and c_0. The In the next time step t = t1, the ship indents into the ice and the ice edge gets crushed. The geometrical parameters then change to θ_1, b_1 and c_1. The meta-model obtained as the product of this section then acts as the function to link the force and geometrical parameters to the outputs $\sigma_{MaxPrinc}$ and l_b. From this, $\sigma_{MaxPrinc}$ and l_b are obtained as functions of the indentation depth, which can be transformed to time histories according to the indentation speed.

The model is set up with model-scale ice thickness (h = 3 cm) and elastic modulus (E = 50 MPa). The results can be scaled for any ice thickness and elastic modulus according to the derivation in Appendix I. The normal force exerted on the contact area is set with uniform pressure 1 kPa. The material is set as pure elastic so the stress is linearly dependent on the pressure in the contact area, thus can be directly scaled. The presented parameterization allows simplification of the problem while keeping the main features of the problem as identified in Section 4, and controlling of the problem with five inputs and two outputs, making the problem suitable for meta-modeling.

Table 3
Parameter values for simulation.

Parameter	Range	Number
θ	[10, 40, 70, 100, 130, 160] deg	6
b	[6, 15, 30, 60, 120, 240, 360, 480, 600]mm	9
c	[15, 30, 60, 120, 180, 240, 300, 360, 420]mm	9
μ_1	[0.05, 0.1, 0.15, 0.2]	4
μ_2	[0.05, 0.1, 0.15, 0.2]	4

5.2. Generation of a database

With the above parameterization, a database is to be built via FE simulations in order to get a large number of samples for fitting. The FE model is set the same as the model in Section 4, but excludes the crack simulation. The automation is achieved through Python scripting. A loop is set in the Python script to execute the simulation with each combination of the five input parameters. Each model is then automatically set up and meshed according to defined meshing strategy. The element sizes are set to be dependent on the geometrical parameters θ, b, c. The discrete range of input parameters are listed in Table 3. The range is set to cover practically reasonable scenarios. All together $6 \times 9 \times 9 \times 4 \times 4 = 7776$ simulations are run. The running time of each simulation varies approximately from 15 s to around 1 min for a normal PC depending on the cases. After all the result files are obtained, another Python script is written to automatically extract the bending stress on the top layer and its location. The computation is conducted with five jobs running in parallel, which takes approximately 12 h to establish the database. Finally, a result matrix with all the input and output information is obtained.

5.3. Database fitting with neural network

It is not straightforward to find the best way to fit the simulation database. In this problem, there are five input variables and two output variables. The optimal function to fit the data cannot be visually estimated by simply plotting all the variables in a figure. Advanced fitting techniques are called for to fit the result with good accuracy.

The model used in this paper is a two-layer non-linear neural network, illustrated in Fig. 9. Ten neurons are used for each layer. More neurons may improve the fitting performance but meanwhile increase the likelihood of overfitting. The essence of the neural network fitting is to fit the database with the following function:

$$y = W_2 \cdot \mathscr{S}(W_1 X + b_1) + b_2 \tag{1}$$

where $\mathbf{W_1}$ and $\mathbf{W_2}$ are the weights, with dimensions of 10×5 and 10×1 respectively; $\mathbf{b_1}$ and $\mathbf{b_2}$ the bias; $\mathbf{X}$ the normalized input vectors and y the normalized output. $\mathscr{S}$is the sigmoid function accounting for the non-linear relationships.

The fitting is conducted through the neural network fitting toolbox in Matlab. The database is separated into 80% training set, 10% validation set and 10% test set. Fig. 10 and Fig. 11 show the fitting performance. For the model fitting of the maximum principal stress, the R-value is as high as 0.998 in all the three sets, with most of the points spreading very close to the line Y = T, indicating that the neural network can fit the result with excellent performance. For the model fitting of the location of maximum stress, the performance is not as excellent as that for maximum stress, but still gives R value as high as 0.980. The points also spread along Y = T but with slightly larger variation.

5.4. Simulation of ship-ice interaction with the derived neural network

The fitted neural network needs negligible computation time and gives σMaxPrinc and lb directly from the input vector. In the next step, the fitting performance is re-checked in another way. Consider the ship-ice contact scenario illustrated in Fig. 8. As described in the beginning of this section, the input parameters b, c, θ (see Fig. 5a) change as a function of the indentation. Then σMaxPrinc and lb change in the process, which can be calculated with the developed neural network. Therefore, σMaxPrinc and lb can be obtained as functions of the indentation depth. A comparison is made between the predicted σMaxPrinc and lb with neural network and the calculated values from the FE simulation. To avoid subjectivity in selection of the initial parameters, the initial parameters θ_0, b0 together with μ_1 and μ_2 are randomly generated. The initial contact length c0 is set as a small value 0.5 h without losing generality, since c increase as the indentation progresses. Here 25 random cases are plotted in Fig. 12 for a visual check of the fitting to the database. All the parameters are non-dimensionalized. The solid line is the calculation by neural network and the circles are the data read from the database of FE calculation results. It is shown that in most of the cases the neural network gives very close results compared to the simulation data, and in all cases the predicted curve changes smoothly without overfitting. This means that the derived neural network gives rationally sensible and sufficiently accurate results, thus it can replace the FE simulation for practical

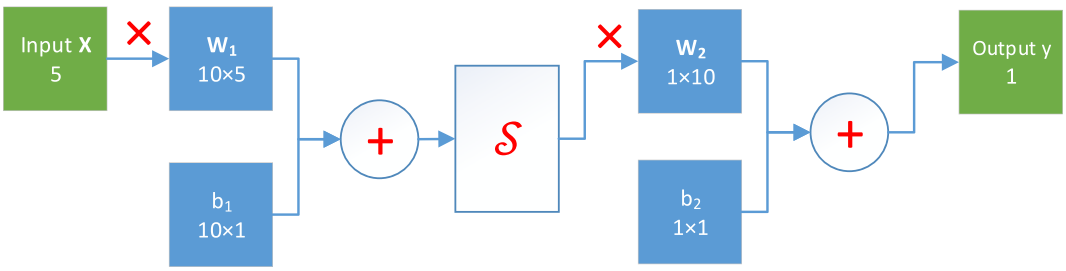

Fig. 9. Graphical illustration of the neural network. The red symbols denote operations; green blocks the input and output; blue blocks the parameters to be learnt. The numbers are the dimensions. (For interpretation of the references to colour in this figure legend, the reader is referred to the Web version of this article.)

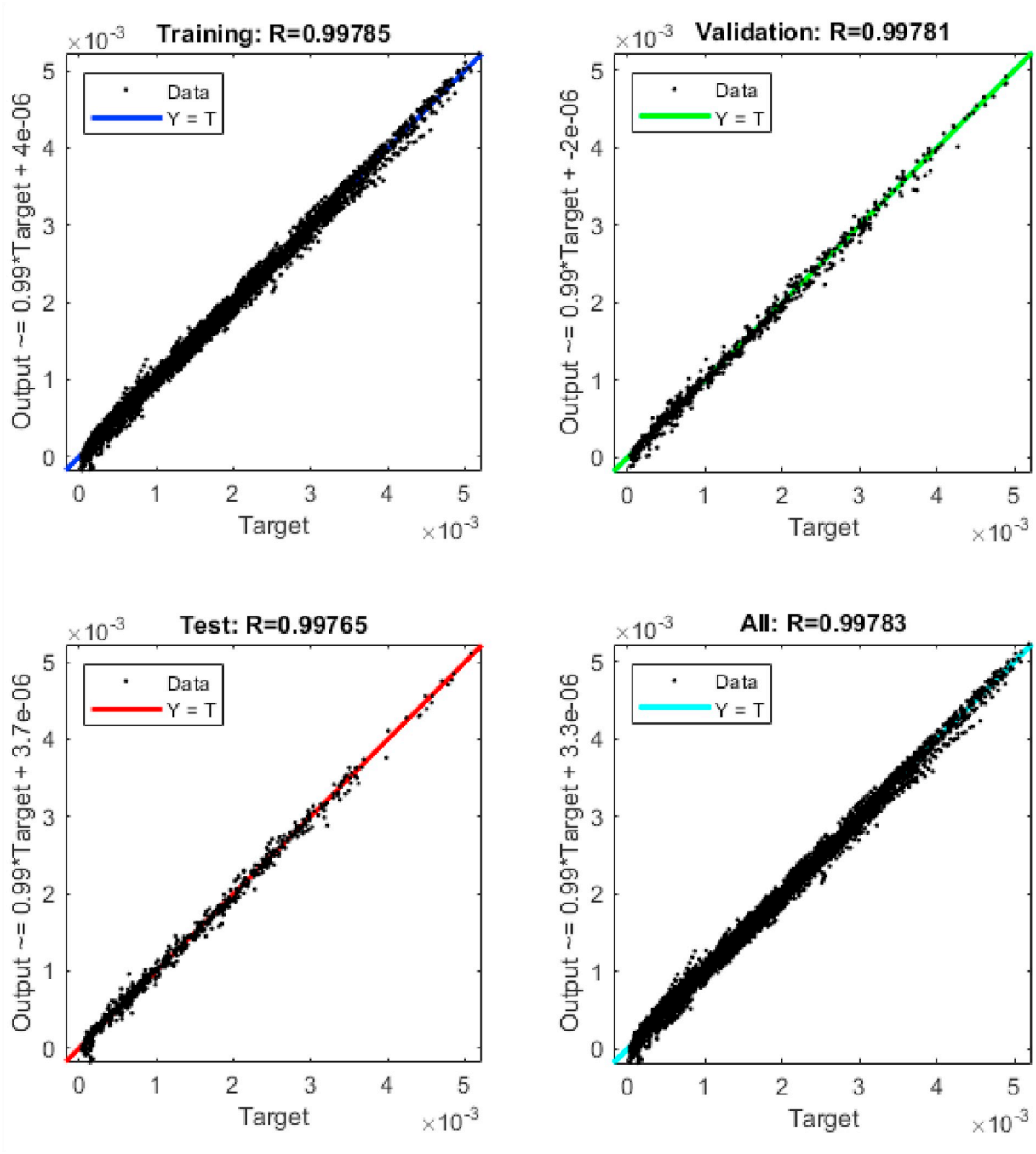

Fig. 10. Neural Network fitting performance on maximum principal stress.$\sigma_{MaxPrinc}$

implementation in a ship performance model.

6. Uncertainty due to variation of ice property along thickness

The previous section used homogeneous elastic modulus for modelling. However, as already pointed out by Kerr and Palmer [34], the actual elastic modulus profile through thickness has a major effect on the bending stress. The elastic (or strain) modulus of model ice [35] and sea ice [36,37] at the top layer is usually higher than in the bottom layer. This section aims to quantify the uncertainty arising from the idealization of the ice sheet as homogeneous material, in order to add more insights to the results of the previous section.

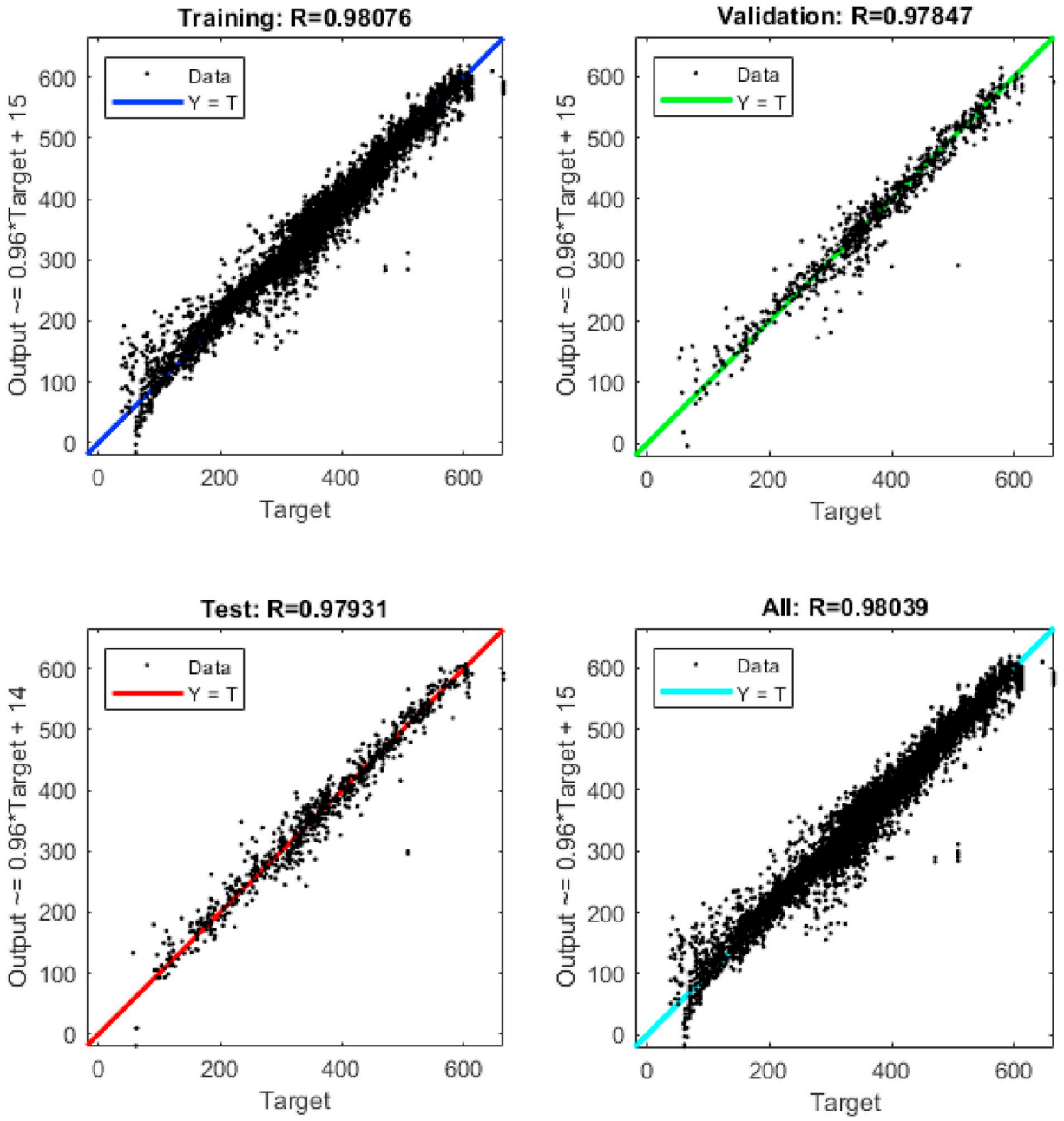

Fig. 11. Neural Network fitting performance on the breaking length *lb*.

6.1. *Modeling the uncertainty*

6.1.1. *Modelling elastic modulus profile through thickness*

A power function was applied by von Bock und Polach [35] to represent the elastic modulus gradient through thickness, with the assumption that the elastic modulus at the top layer is seven times of the mean through the thickness. However, the equation needs a definition of the top layer thickness. In this paper, the elastic modulus profile is modelled with an exponential function as follows

$$E(h) = E_{top} e^{-bh} \tag{2}$$

Denoting the elastic modulus in the top layer E_{top}, which equals *r*times the mean elastic modulus E_{mean}through the thickness, the coefficient b can be easily solved as a function of *r*. As shown in Fig. 13, when $r < 2$, it is approximately a linear function; when $r = 1$, b becomes zero and *E(h)* becomes a constant. The elastic modulus variation becomes significant when r is larger than 4.

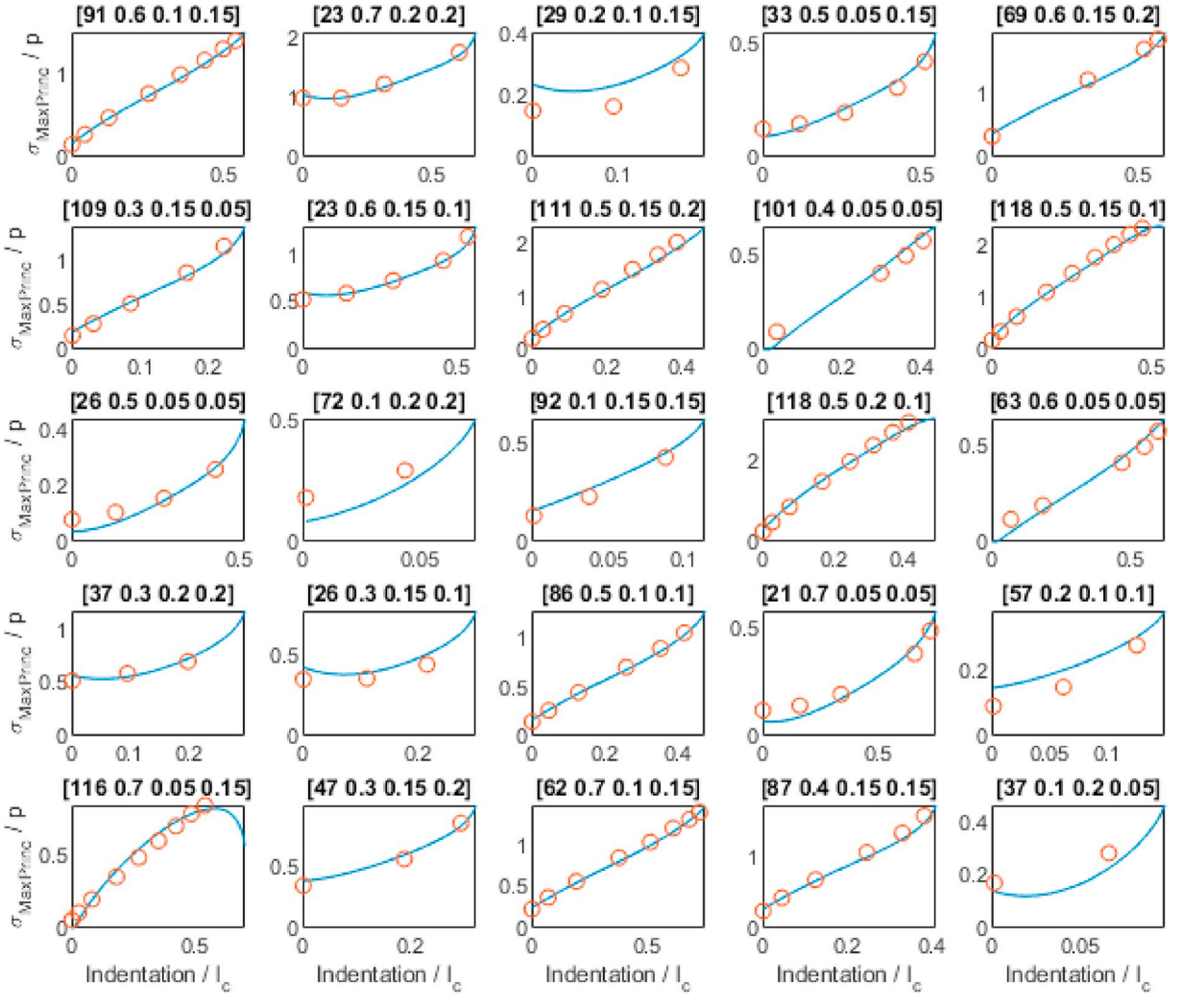

Fig. 12. Stress-indentation curve (a) and breaking length-indentation curve (b) of 25 random cases. The circles are the values from the database calculated by FE simulation; the solid lines are the predicted results by the neural network. The numbers in the title corresponds to $[\theta_0, b_0/l_c, \mu_1, \mu_2]$.

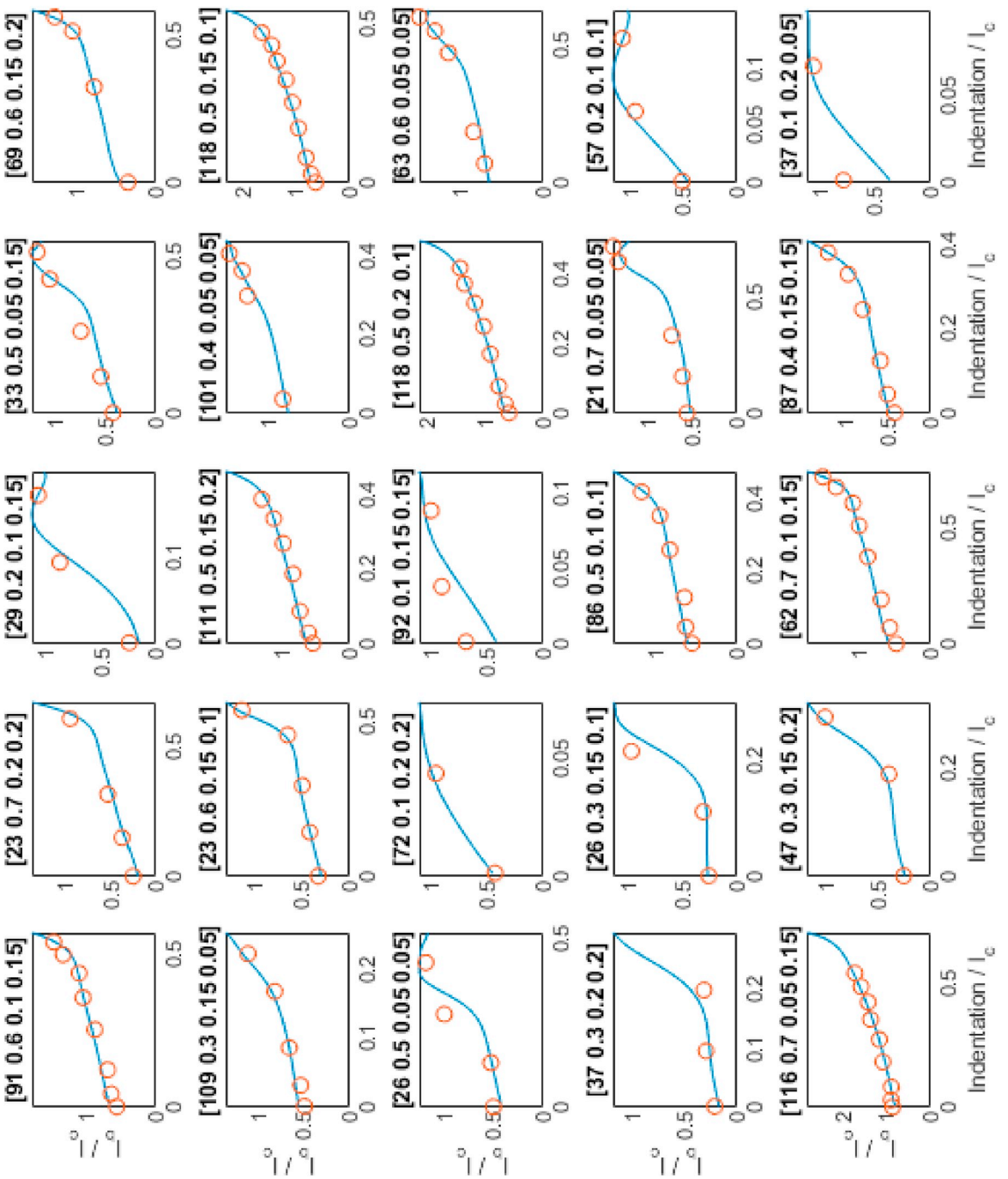

(b)

Fig. 12. (*continued*).

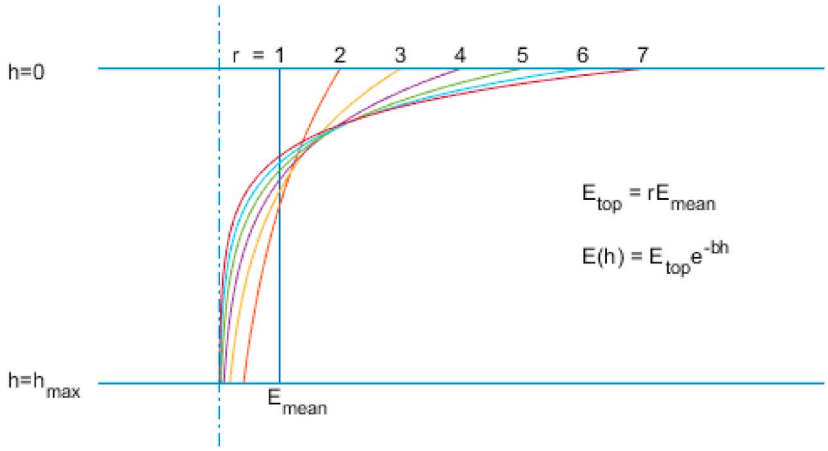

Fig. 13. Elastic modulus gradient with different r according to Eq. (2).

6.1.2. Variation of results with different modulus profile

The same set-up as in Section 5 are adopted here. The ice sheet is modelled with eight layers of elements through the thickness, each assigned an elastic modulus calculated via Eq. (2), which equals the mean elastic modulus of this layer. The elastic modulus in the model therefore follows a piecewise constant function. In the next step, from Table 3, 100 cases are randomly generated with different combinations of the inputs. Each case is then run with r varying from 2 to 5, in total yielding 400 results. Similarly, the bending stress and its location are extracted, and here denoted as σ_r and l_{br} for $r \in [2, 3, 4, 5]$.

Fig. 14 presents the results. The homogeneous cases (r = 1) are used as the reference values and the results are plotted in terms of σ_r/σ_1 and l_{br}/l_{b1}. The mean values are plotted together with the standard deviation, as functions of r. It shows that the stress increases with larger r while l_b decreases. In terms of the mean value, the ratio of σ_r/σ_1 already reaches 2 when r equals 2 and can be as high as 8 when r equals 5. On the contrary, the ratio of breaking length l_{br}/l_{b1} decrease significantly when r changes from 1 to 3 and gets asymptotic to approximately 0.6 with higher r.

6.1.3. Normalized variation of results with different modulus profile

The uncertainty seems to be dramatic based on Fig. 14. However, the uncertainty can be normalized by corrected flexural strength for practical use, making the uncertainty less significant. In modelling ice bending failure, the most important index is the relative magnitude between the bending stress in the ice sheet (here σ_r) and the limit stress $\sigma_f$which the ice can bear, i.e. $\sigma_r/\ \sigma_f$. By comparing

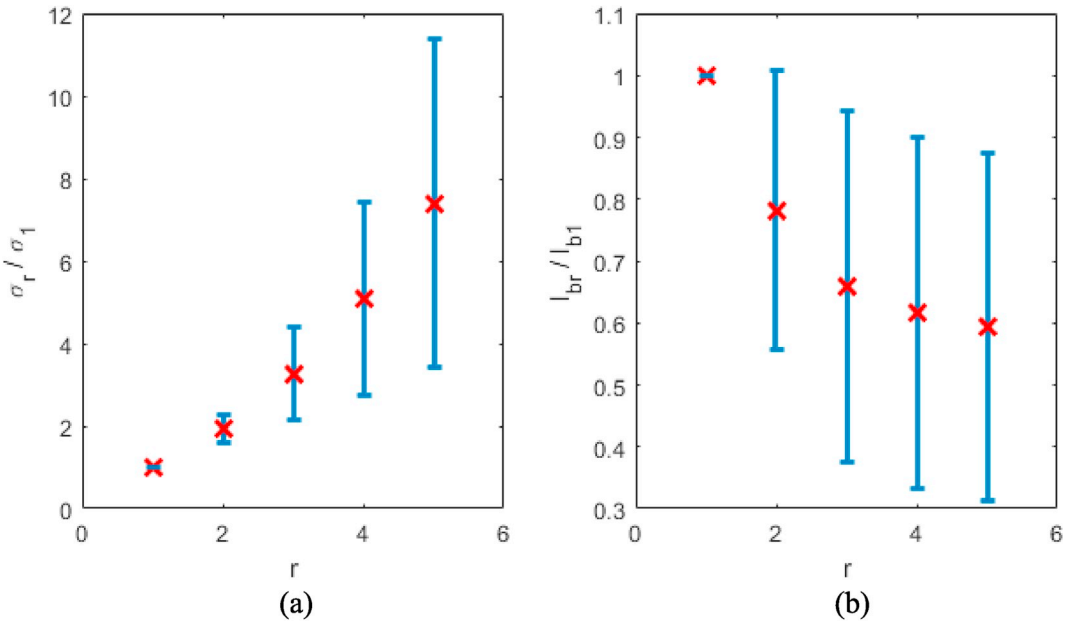

Fig. 14. Mean and standard deviation of the relative difference in σ and l_b as functions of r. The results with $r = 1$ are obtained from the simulations in Section 5 and presented here for comparison.

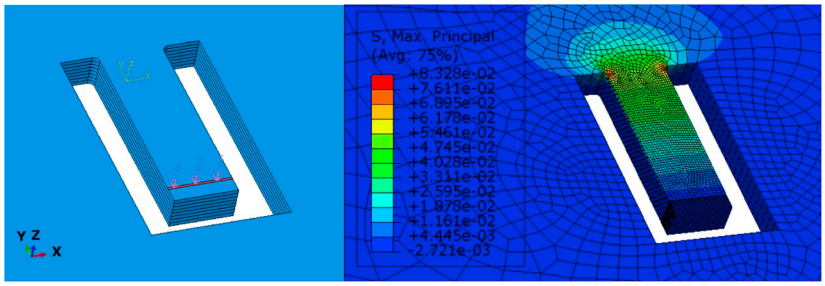

Fig. 15. FE model of cantilever beam test. Left: force on the beam; Right: distribution of maximum principal stress.

Table 4
Corrected flexural strength with different r under unit force.

r	1	2	3	4	5
$\sigma_{fr}/\ \sigma_{f1}$ [a]	1	1.51	2.03	2.61	3.27

[a] $\sigma_{f1}\ = 25.0kPa$

this ratio to 1, it tells whether bending failure happens. The flexural stress is a widely used engineering index to define the limit stress [22]. It is normally calculated by beam theory according to the maximum force exerted on a cantilever ice beam or a three-point or four-point bending beam [38]. This is based on the assumption of constant elastic modulus. With an elastic modulus gradient, the obtained limit strength (here denoted as σ_{fr}) should also be modified.

To address this effect, cantilever beam tests are calculated with different elastic modulus distribution as Fig. 13 presents. The configuration of the simulation is shown in Fig. 15. The size of the beam is set as 175 mm in length, 60 mm in width and 30 mm in thickness in accordance to ITTC [38]. A unit force is exerted on a line 15 mm from the free edge [35]. The obtained bending stresses with different r are listed in Table 4. Here the absolute values does not matter but the ratio $\sigma_{fr}/\sigma_{f1}$is in focus. In all cases, the bending stress occurs at the root of the beam. Similar to Fig. 14, σ_{fr}also increase with larger r, but less significantly. This obtained $\sigma_{fr}/\ \sigma_{f1}$can be used to correct the obtained flexural strength for a beam with varying elastic modulus.

Fig. 14a can now be normalized by changing the y-axis to $\frac{\sigma_r}{\sigma_{fr}}/\frac{\sigma_1}{\sigma_{f1}}$, presented in Fig. 16. With the correction of flexural strength, the uncertainty is significantly reduced, with the ratio of about 2.2 when r = 5. Combined with Fig. 14b, it can be summarised that when r $<$ 2, the relative difference both in terms of stress and breaking length are within 30%, therefore the deviation is still acceptable. When r is larger than 3, the difference is noticeable and the influence must be considered. The mean value of $\frac{\sigma_r}{\sigma_{fr}}/\frac{\sigma_1}{\sigma_{f1}}$can be nicely fitted with a linear function $y\ = 0.3x + 0.7$.

6.2. *Applying the uncertainty evaluation*

Finally, the results of the proposed ship-ice interaction model can be expressed in the following way. As illustrated in Fig. 8, the

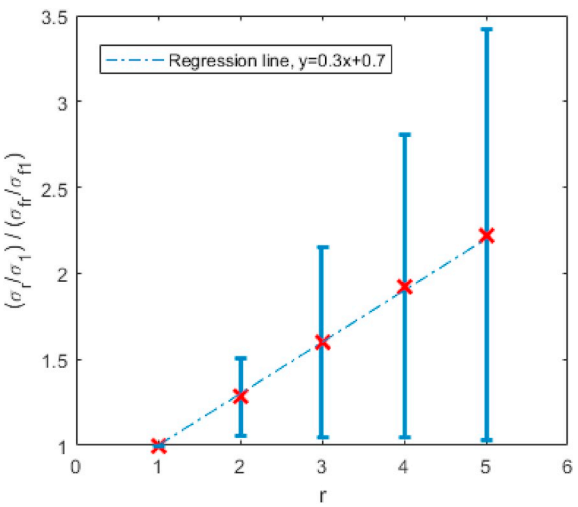

Fig. 16. Normalized mean and standard deviation of the relative difference in.σ

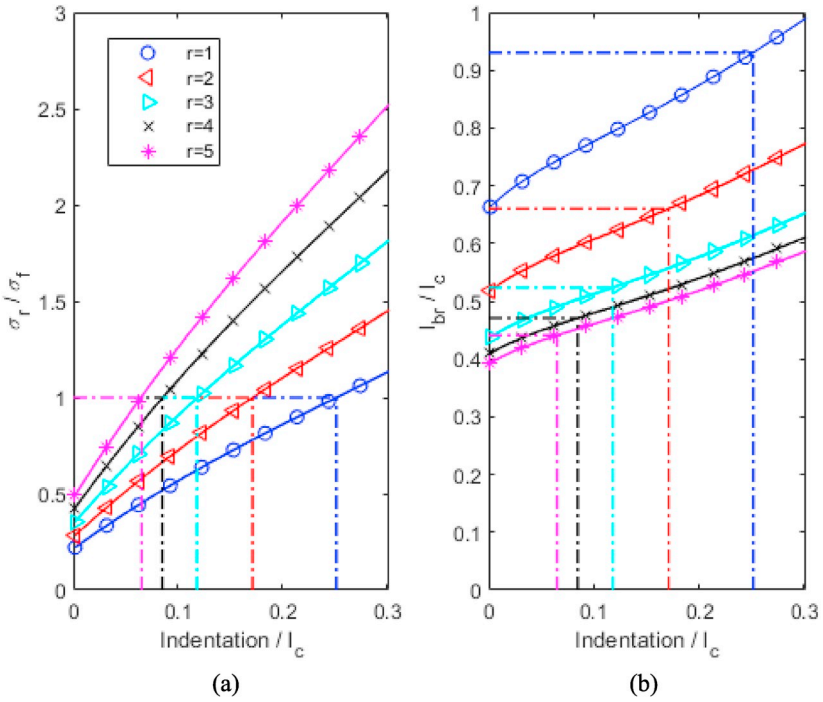

Fig. 17. Example of applying the uncertainty quantification with varying r.

input parameters of the neural network is a function of the initial parameters and the indentation, while the indentation is a function of time depending on indentation speed, i.e.

$$\left[\theta, \frac{b}{l_c}, \frac{c}{l_c}, \mu_1, \mu_2\right] = f\left(\theta_0, \frac{b_0}{l_c}, \frac{c_0}{l_c}, \mu_1, \mu_2, ind(t)\right) \tag{3}$$

The bending stress and potential breaking length are calculated from the neural network:

$$\sigma_1(ind(t)) = \mathrm{NN}_1\left(\theta, \frac{b}{l_c}, \frac{c}{l_c}, \mu_1, \mu_2\right), \quad l_{b1}(ind(t)) = \mathrm{NN}_2\left(\theta, \frac{b}{l_c}, \frac{c}{l_c}, \mu_1, \mu_2\right) \tag{4}$$

where NN denotes the obtained neural networks. With estimated r, the bending failure happens at $t = t_f$, when

$$\frac{\sigma_r}{\sigma_{fr}} \geq 1, \quad where \ \frac{\sigma_r}{\sigma_{fr}} = \frac{\sigma_1}{\sigma_{f1}} \times \left(\frac{\frac{\sigma_r}{\sigma_{fr}}}{\frac{\sigma_1}{\sigma_{f1}}}\right) = \frac{\sigma_1}{\sigma_{f1}} \times (0.3r + 0.7) \tag{5}$$

Here σ_{f1} is obtained from e.g. a cantilever beam test. The breaking length l_{br} when bending failure happens is then

$$l_{br} = l_{b1}(t_f) \times (l_{br} / l_{b1}) \tag{6}$$

where l_{br}/l_{b1} is obtained from Fig. 14b.

An example of applying the uncertainty evaluation results is given using the first case in Fig. 12. Fig. 12 presented the results of σ_1 and l_{b1} until Eq. (4). With Eq. (5), taking the flexural strength when r = 1 (i.e. σ_{f1}) as 0.75p as an example, $\frac{\sigma_r}{\sigma_{fr}}$ are plotted in Fig. 17 as functions of the indentation depth with different r values. The horizontal dash-dot lines represent the threshold $\frac{\sigma_r}{\sigma_{fr}} = 1$, which corresponds to the critical indentation depth leading to bending failure. The obtained indentation values in this case are 0.25, 0.17, 0.12, 0.084, 0.065 respectively for r equaling 1 to 5. The same can be plotted in Fig. 17b in terms of the breaking length based on Eq. (6). From the indentation which leads to bending failure obtained from Fig. 17a, the breaking length corresponding to these indentations at different r values can be found by the dash-dot lines. In this case, the breaking lengths l_b/l_c are found to be 0.93, 0.66, 0.52, 0.47, 0.44 respectively for r equaling 1 to 5.

7. Discussion on the modelling process

The previous sections presented a systematic approach to model the ice bending failure at ships' shoulder and midship area where the in-plane force is much larger than out-of-plane force, in the context of a cross-scale problem. It starts with observations in full-scale

and model-scale to identify the key issues, followed by numerical simulations to capture the phenomena (Section 4). A meta-modelling approach is applied through neural network fitting to obtain an analytical expression for prediction of bending failure (Section 5). Finally, the uncertainty is quantified to model the deviation due to an important simplification in the modelling process (Section 6). Compared to conventional modelling approaches for such kind of problems, there are two new features in this approach which improves the modelling performance to a higher level.

The first feature is the meta-modelling approach, realized by adopting advanced fitting technique to a database of results generated by FE modelling. The obtained neural network takes negligible time in computation while maintaining the accuracy level as high as numerical calculation. Such model is suitable for modelling in global scale which, in this context, is the ship performance in ice. The model is compatible with most of the existing simulation models, e.g. Lubbad and Løset [3]; Su et al. [11]; Li et al. [27], thus can be directly applied to these models without major modification, while providing more accurate modelling of ship-ice interaction. The same approach may be extended to model the ship-ice interaction at bow area, but the hydrodynamic effect may need to be properly dealt with.

The second feature is the uncertainty modelling. Due to lack of knowledge in ice mechanics, even the most complicated model cannot give robust predictions on the macroscopic behavior of ice. Ice-related models are usually questioned due to the set parameters or coefficients which cannot or have not been systematically verified, e.g. by experiment. Due to these, a principle is followed while developing this model, that least subjectivity should be involved. The model is thus developed with homogeneous elastic material, and with measured flexural strength as the strength limit. Features such as the modulus gradient through thickness are known to exist, but are difficult to quantify. This feature is then modelled by uncertainty analysis to quantify the deviation it may lead to the predictions. Uncertainty analysis is an indispensable element to complete a model, where certain important simplifications and assumptions are inevitably needed.

However, ice is known to be more complex than pure elastic. There can be at least viscous elastic and delayed elastic behavior meanwhile [22]. The ice in model scale may be very plastic [35]. The uncertainties arising from these components are expected to be more complex to evaluate, and the extent of their influence to the problem in ship scale is yet unknown. Therefore, the model in this paper is under the assumption that modelling the pure elastic behavior can give a reasonable approximation to the actual ice bending behavior. It should be also noticed that the developed model only deals with the stress evolvement until crack initiation, while the crack propagation is only qualitatively investigated. The crack propagation demands additional energy and leads to higher load. This should be given more attention when dealing with ice bending problems.

The current model is obtained by one set of ice thickness and elastic modulus. The scaling laws in Appendix I can be used for different ice thickness and elastic modulus. The scaling laws are derived from plate theory so it should be used with scrutiny for very thin or very thick ice. However, one can run a much larger database and fit new neural networks by FE simulations with varying ice thickness and elastic modulus following the same approach, if he aims for the most accurate solution. This takes much more time to build the database, but is still possible to do, especially considering this only has to be conducted once.

8. Summary and conclusions

To summarize, this paper proposed a novel approach to model ship-ice interaction, in order to be applied into ship scale simulations. The XEFM-based simulation provides insights to the observed failure mode. The FE based meta-modelling approach proves its excellent capability for cross-scale modelling in maintaining the high accuracy with negligible computational power. The uncertainty quantification enables effectively accounting for the elastic modulus profile through thickness. Based on the results and discussions, the following conclusions are drawn:

1. The XFEM simulation gives hints that considerable additional energy is needed to break through the ice when there is large in-plane force.
2. Neural network fitting gives excellent fitting performance to a database of ice failure cases. It can act as a powerful fitting tool nowadays when extensive data becomes available both from simulation and from measurement.
3. Uncertainty due to the modulus gradient through thickness should not be simply neglected, especially when the modulus at the top layer is over three times of the mean modulus. This paper provide a convenient way to account for this uncertainty.

As for future work, the results of this paper will be implemented into ship scale models to simulate ship performance. The model is then simulation-free in ship-ice interaction scale, but maintains the accuracy meanwhile.

Acknowledgement

This work has received funding from the South-eastern Finland–Russia CBC 2014–2020 program via the project Future Potential of Inland Waterways (INFUTURE, funding number KS1006). The contributions by last author were supported in part thanks to funding from the Canada First Research Excellence Fund, through the Ocean Frontier Institute.

Appendix I Supplementary material

The obtained neural network functions are attached as the supplementary material in Matlab m-file.

Appendix II. Scaling of the results

The inputs and outputs in the results have been expressed in Section 5 in terms of non-dimensional parameters θ, b/l_c, c/l_c, μ_1, μ_2, $\sigma MaxPrinc/p$ and l_b/l_c, with the elastic modulus set as 50 MPa and ice thickness 30 mm. The elastic modulus and ice thickness are not varied in the simulations because these can be reasonably accounted for analytically according to the scaling laws presented in this appendix. The number of simulations needed to run is then significantly reduced with two fewer parameters to compute.

The linearity in the modelling process enables the scalability of the obtained results. The scaling laws are derived according to an analogy to plate theory. As already demonstrated by several previous papers, e.g. Li et al. [27] and Nevel [32], a Kirchhoff-Love plate (or Euler-Bernoulli beam) resting on elastic foundation can be non-dimensionalized by the characteristic length lc. Therefore, the coordinate system χ-γ can be non-dimensionalized. For a Kirchhoff-Love plate resting on elastic foundation, the stress $\sigma 1$ at a non-dimensionalized location ($\chi 1$, $\gamma 1$) caused by a unit force at ($\chi 2$, $\gamma 2$) is proportional to h-2. Additionally, $\sigma 1$ is a function of the force magnitude, which is then the product of nominal pressure p and contact area A. The contact area A is equal to h times c, which finally yields the following scaling relationship:

$$\sigma \propto h^{-2} * p * A = h^{-2} * p * h * c \propto p * h^{-1} * l_c \propto p * h^{-1} * E^{0.25} * h^{0.75} = \frac{p * E^{0.25}}{h^{0.25}} \tag{I.1}$$

The pressure p can be set as a constant or area-independent according to the user. The scaling of the breaking length l_b is straightforward since l_b/l_c is a non-dimensional length parameter, and therefore remains unchanged in scaling.

The validity of the relationship can be easily validated. As an example, the same inputs [θ, b/l_c, c/l_c, μ_1, μ_2] = [100deg, 0.36, 0.36, 0.1, 0.1] are applied for two additional simulations with the same configuration in Section 5, but with full-scale parameters. The parameters together with the simulated and scaled results are listed in Table I.1. The deviations compared to the scaled results are rather small, indicating that the above scaling laws derived from plate theory can still give good approximations to the results calculated from FE using solid elements.

Table I.1
Examples of results scaling

Case	[h, E]	Simulated	Scaled from reference
Reference	[30 mm, 50 MPa]	[0.805 kPa, 303 mm]	
1	[300 mm, 5 GPa]	[1.62 kPa, 4860 mm]	[1.43 kPa, 5388 mm]
2	[600 mm, 2 GPa]	[1.00 kPa, 6814 mm]	[0.957 kPa, 7206 mm]

References

[1] Lindqvist G. A straightforward method for calculation of ice resistance of ships. In: Proc. 10th int. Conf. Port ocean eng. Under arct. Cond. Sweden: Luleå; 1989.
[2] Riska K, Wilhelmson M, Englund K. Performance of merchant vessels in ice in the Baltic. Tech. Rep. Report 52. Winter Navigation Research Board; 1997.
[3] Lubbad R, Løset S. A numerical model for real-time simulation of ship–ice interaction. Cold Reg Sci Technol 2011;65:111–27.
[4] Li F, Goerlandt F, Kujala P, Lehtiranta J, Lensu M. Evaluation of selected state-of-the-art methods for ship transit simulation in various ice conditions based on full-scale measurement. Cold Reg Sci Technol 2018;151:94–108.
[5] Gong H, Polojärvi A, Tuhkuri J. Preliminary 3D DEM simulations on ridge keel resistance on ships. In: Proc. 24th int. Conf. Port ocean eng. Under arct. Cond.; June 2017. Busan, Korea.
[6] Sorsimo A, Nyman T, Heinonen J. Ship-ice interaction in a channel. Tech. Rep. Report 93. Winter Navigation Research Board; 2016.
[7] Lubbad R, Løset S, Lu W, Tsarau A, van den Berg M. Simulator for arctic marine structures (SAMS). In: Proc. ASME 2018 37th int. Conf. Ocean. Offshore arct. Eng. (OMAE2018), Madrid, Spain; 2018.
[8] Kuuliala L, Kujala P, Suominen M, Montewka J. Estimating operability of ships in ridged ice fields. Cold Reg Sci Technol 2017;135:51–61.
[9] Lehtola V, Montewka J, Goerlandt F, Guinness R, Lensu M. Finding safe and efficient shipping routes in ice-covered waters: a framework and a model. Cold Reg Sci Technol 2019;165.
[10] Kujala P, Goerlandt F, Way B, Smith D, Yang M, Khan F, et al. Review of risk-based design for ice-class ships. Mar Struct 2019;63:181–95.
[11] Su B, Riska K, Moan T. A numerical method for the prediction of ship performance in level ice. Cold Reg Sci Technol 2010;60:177–88.
[12] Haapala J, Lönnroth N, Stössel A. A numerical study of open water formation in sea ice. J Geophys Res C Oceans 2005;110:1–17.
[13] Valtonen V. Effect of rudder force on stern shoulder region ice loads. Arct. Technol. Conf. 2016:24–6.
[14] Liu J, Lau M, Williams F. Mathematical modeling of ice-hull interaction for ship maneuvering in ice simulations. Icetech 2006;1–8.
[15] Kulaots R, Kujala P, von Bock und Polach RUF, Montewka J. Modelling of ship resistance in compressive ice channels. In: Proc. 22nd int. Conf. Port ocean eng. Under arct. Cond., espoo, Finland; 2013.
[16] Kolari K. A complete three-dimensional continuum model of wing-crack growth in granular brittle solids. Int J Solid Struct 2017;115–116:27–42.
[17] Liu Z, Amdahl J, Løset S. Plasticity based material modelling of ice and its application to ship–iceberg impacts. Cold Reg Sci Technol 2011;65:326–34.
[18] Xu Y, Hu Z, Ringsberg JW, Chen G. Nonlinear viscoelastic-plastic material modelling for the behaviour of ice in ice-structure interactions. Ocean Eng 2019;173:284–97.
[19] Lu W, Lubbad R, Løset S. Out-of-plane failure of an ice floe: radial-crack-initiation-controlled fracture. Cold Reg Sci Technol 2015;119:183–203.
[20] Lu W, Lubbad R, Løset S. In-plane fracture of an ice floe: a theoretical study on the splitting failure mode. Cold Reg Sci Technol 2015;110:77–101.
[21] Lu W, Lubbad R, Løset S, Høyland KV. Cohesive zone method based simulations of ice wedge bending: a comparative study of element erosion, CEM, DEM and XFEM. 21st IAHR Int Symp Ice 2012:920–38.
[22] Timco GW, Weeks WF. A review of the engineering properties of sea ice. Cold Reg Sci Technol 2010;60:107–29.
[23] Dempsey JP, Adamson RM, Mulmule SV. Scale effects on the in-situ tensile strength and fracture of ice Part I: large grained freshwater ice at Spray Lakes Reservoir, Alberta - Springer. Int J Fract 1999;95:347–66.

[24] Zhou L, Riska K, Moan T, Su B. Numerical modeling of ice loads on an icebreaking tanker: comparing simulations with model tests. Cold Reg Sci Technol 2013; 87.
[25] Suominen M, Karhunen J, Bekker A, Kujala P, Elo M, von Bock und Polach R, et al. Full-scale measurements on board PSRV S.A. Agulhas II in the Baltic Sea. Port Ocean Eng under Arct Cond 2013.
[26] Kotilainen M, Vanhatalo J, Suominen M, Kujala P. Predicting ice-induced load amplitudes on ship bow conditional on ice thickness and ship speed in the Baltic Sea. Cold Reg Sci Technol 2016;135:116–26.
[27] Li F, Kotilainen M, Goerlandt F, Kujala P. An extended ice failure model to improve the fidelity of icebreaking pattern in numerical simulation of ship performance in level ice. Ocean Eng 2019;176:169–83.
[28] Li F, Kujala P, Montewka J. A ship in compressive ice: an overview and preliminary analysis. In: Proc. 25th int. Conf. Port ocean eng. Under arct. Cond. Delft, Netherl.; 2019.
[29] Belytschko T, Moës N, Dolbow J. A finite element method for crack growth without remeshing. Int J Numer Methods Eng 1999;46:131–50.
[30] Valanto P. On the cause and distribution of resistance forces on ship hulls moving in level ice. In: Proc 18th int. Conf. Port ocean eng. Under arct. Cond.; 2001.
[31] Keijdener C, Hendrikse H, Metrikine A. The effect of hydrodynamics on the bending failure of level ice. Cold Reg Sci Technol 2018;153:106–19.
[32] Nevel DE. The theory of a narrow infinite wedge on an elastic foundation. Trans Eng Inst Canada 1961;2:132–40.
[33] Varsta Varsta, Petri. On the mechanics of ice load on ships in level ice in the Baltic Sea, vol. 11. Technical Research Centre of Finland, VTT, Publications; 1983. p. 91.
[34] Kerr AD, Palmer WT. The deformations and stresses in floating ice plates. Acta Mech 1972;15:57–72.
[35] von Bock und Polach RUF. Numerical analysis of the bending strength of model-scale ice. Cold Reg Sci Technol 2015;118:91–104.
[36] Ehlers S, Kujala P. Optimization-based material parameter identification for the numerical simulation of sea ice in four-point bending. Proc Inst Mech Eng Part M J Eng Marit Environ 2014;228:70–80.
[37] Idrissova S, Kujala P, Repin R, Li F. The study of the Popov method for estimation of ice loads on ship ' s hull using full -scale data from the Antarctic sea. In: Proc. 25th int. Conf. Port ocean eng. Under arct. Cond. Delft, Netherl.; 2019.
[38] Ittc ITTC. Recommended procedures ITTC – test methods for model ice properties. ReVision 2014:266–73.